Ligand-to-Metal Charge Transfer Resulting in Metalloaromaticity of [R,R-Cyclohexyl-1,2-bis(2-Oxidonaphthylideneiminato-N,N′,O,O′)]Cu(II): A Scrutinized Structural Investigation

ARTICLE *in* JOURNAL OF INORGANIC AND ORGANOMETALLIC POLYMERS AND MATERIALS · APRIL 2010

Impact Factor: 1.16 · DOI: 10.1007/s10904-009-9323-3

J Inorg Organomet Polym (2010) 20:142–151
DOI 10.1007/s10904-009-9323-3

Ligand-to-Metal Charge Transfer Resulting in Metalloaromaticity of [*R,R*-Cyclohexyl-1,2-bis (2-Oxidonaphthylideneiminato-*N,N′,O,O′*)]Cu(II): A Scrutinized Structural Investigation

Hasan Karabıyık · Özlem Erdem · Muhittin Aygün · Bilgehan Güzel · Santiago García-Granda

Received: 4 November 2009 / Accepted: 24 December 2009 / Published online: 7 January 2010

Abstract Molecular and crystal structure analysis of a tetradentate ligand-to-metal charge transfer (LMCT) complex, [*R,R*-cyclohexyl-1,2-bis(2-oxidonaphthylideneiminato-*N,N′,O,O′*)]Cu(II), are described and characterized by X-ray crystallography and FTIR spectroscopy. The Cu(II) centers are coordinated by four atoms of the donor set [N_2O_2] in a distorted square-planar fashion, which can be attributed to an active electronic delocalization within metallacycles and polychelating property of the pro-ligand. Bond valences of copper centers in four crystallographically independent monomers are slightly distinguished from each other, which is associated with differences in charge delocalization levels of the pro-ligands. Total valence of the copper center is increased with increasing π-electron donation from naphthalene fragments to metallacycles. This charge transfer leads to π···π interactions between metallacycles including imine bridges. In addition, decreases in the centroid–centroid distances of π···π interactions are associated with increased aromatic character of metallacycles. Molecules of the complex are stacked as dimers in the crystal structure formed by π···π interactions and aggregations of these dimeric formations along *a*-axis are strengthened by C–H···O type H-bonds and C–H···π interactions.

H. Karabıyık (✉) · M. Aygün
Department of Physics, Dokuz Eylül University, 35160 Buca, İzmir, Turkey
e-mail: hasan.karabiyik@deu.edu.tr

Ö. Erdem · B. Güzel
Department of Chemistry, Çukurova University, 01330 Adana, Turkey

S. García-Granda
Departamento de Química Física y Analítica, Universidad de Oviedo, 33006 Oviedo, Spain

Keywords Metalloaromaticity · Valence tautomerism · *bis*(tetradentate) Schiff base ligand · Ligand-to-metal charge transfer (LMCT) complex · HOMA

1 Introduction

The ground states of salicylaldehyde, salicylaldimine or hydroxy naphthaldimine can be regarded as a resonance hybrid of two canonical structures, phenol-aldehyde state and the protonated quinoid-enolate (zwitterionic) state [1] or quinoid and zwitterionic state [2–5]. This character of their ground states suggests that intramolecular H-bonds in such molecular fragments can easily perturb enhanced stabilization by electronic delocalization along a proton-bridged quasi-six-membered chelate ring involving low-lying vacant *p*-type orbitals on the tautomeric protons [4, 5]. Such H-bonds are classified as resonance [6, 7] or charge assisted [8] hydrogen bonding. Resonance assisted H-bonds (RAHBs) affect the electronic state of its neighboring aromatic fragments [4–8]. When these compounds are used as pro-ligand in an organometallic compound, electronic repulsive and attractive effects between the ligand and metal ion become important. Since π-conjugated molecules having coordination capabilities with metal ions such as Schiff bases are electroactive or redox-active due to π-electronic coupling between the acidic and basic centres of the molecule [7], the electronic state of the metal center may be coupled with that of the ligand's π-electron system, resulting in a phenomenon referred to as valence tautomerism or redox isomerism [9]. Valence-tautomeric complexes are of great importance in single-molecule magnets and spin-crossover complexes for fine-tuning applications such as memory devices or optical switches [10]. On the other hand, electronic delocalization within the metallacycles of such complexes can cause to

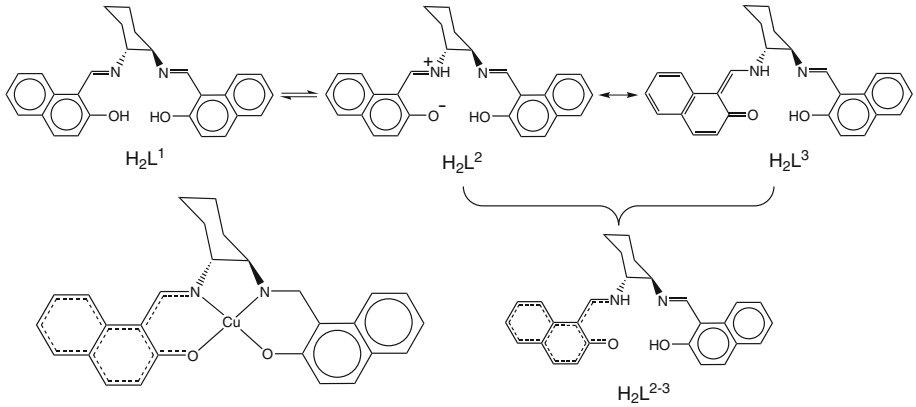

Scheme 1 Tautomeric equilibrium of the pro-ligand (*upper part*) and chemical chart of the title complex (*left lower part*). Dashed lines represent intermediate bond distances

another important phenomenon called as metalloaromaticity [11].

The synthesis, structural and spectroscopic characterization of the pro-ligand of the complex, 1-((*E*)-{(1*R*,2*R*)-2-[(*E*)-(2-hydroxy-1-naphthyl) methyleneamino] cyclohexyl} iminiomethyl) naphthalen-2-olate which can be regarded as a resonance hybrid (H_2L^{2-3}) of H_2L^2 and H_2L^3 in Scheme 1, have already been reported in Ref. [8]. In a continuation of our interest regarding structural and spectral properties of Schiff base complexes, here we report the synthesis and structural characterization of polycyclometallated tetradentate copper(II) Schiff base complex, [*R,R*-Cyclohexyl-1, 2-bis(2-oxidonaphthylideneiminato-*N,N′,O,O′*)]Cu(II), by elemental analysis, FTIR spectroscopy and X-ray crystallography combined with the computational studies. In addition to these, our primary interest will be addressed to examine structure–activity relationship through intramolecular charge transfer with the aid of the calculated valences of Cu centers and aromaticities of certain fragments such as naphthalene and chelate ring. For this purpose, Harmonic Oscillator Model of Aromaticity (HOMA) indices depending only on structural data (bond lengths) are used to estimate π-electron delocalization levels of four different monomers of the complex. Although, at first glance, usage of HOMA index seems to be an improper way to describe directly π-electron delocalization levels in a molecular fragment, it correlates well with *para* delocalization index indicating the amount of sharing π-electrons among atomic centers for polycyclic hydrocarbons such as naphthalene [12].

2 Materials and Methods

2.1 Synthesis of the Complex

A solution of $Cu(OAc)_2/H_2O$ (484 mg, 2.4 mmol) in 40 mL ethanol was added to a solution of the ligand (1-((*E*)-((1*R*, 2*R*)-2-((*E*)-(2-hydroxynaphthalen-1-yl)methyleneamino) cyclohexylimino) methyl)naphthalen-2-olate) (2.4 mmol) in 30 mL ethanol at room temperature. The reaction mixture was stirred for 3 h, at 60 °C to get a dark brown solution. The mixture was concentrated about to 25 mL to precipitate out of complexes from the solution as red solid. The crude product was recrystallized from hexane–dichloromethane mixture. (Yield 92%; m.p. >550 K). Elemental analysis calculated for $C_{28}H_{24}CuN_2O_2$: C, 69.48; H, 5.00; Cu, 13.13; N, 5.79; Found: C, 68.51; H, 4.89; Cu, 13.01; N, 5.83%.

2.2 X-ray Crystallography

Diffraction measurements were performed at 296 K using a Oxford Diffraction Nova diffractometer by CrysAlis CCD [13] and graphite-monochromated CuKα radiation ($\lambda =$ 1.54184 Å). Empirical absorption correction using spherical harmonics implemented in SCALE3 ABSPACK [13] scaling algorithm were applied on the collected data. The structure was solved by using direct methods in WinGX's [14] implementation of SHELXS-97 [15]. In the absence of significant anomalous dispersion effects, 6522 Friedel opposites were merged before final refinement cycle. The scattering factors were taken from SHELXL-97 [15]. Details for the data collection conditions and parameters of refinement process are summarized in Table 1. Further information of crystallographic study may be found in supporting information file.

2.2.1 Supporting Information

Crystallographic data excluding structure factors for the structures reported in this article have been deposited with the Cambridge Crystallographic Data Centre as supplementary publication numbers CCDC 753090. Copies of the data can be obtained free of charge on application to CCDC, 12 Union Road, Cambridge CB2 1EZ, UK (Fax: (+44) 1223 336-033; e-mail: data_request@ccdc.cam.ac.uk).

3 Computational Procedures

The geometry optimization of the title complex leading to energy minima in vacuo were performed by using DFT

Table 1 Crystal data and details of the structure refinement for the title complex

Crystal data	
Chemical formula	$C_{28}H_{24}CuN_2O_2$
M_r	484.03
Crystal system, space group	Triclinic, $P1$
Temperature (K)	296
Crystal size (mm)	0.22 × 0.02 × 0.02
a, b, c (Å)	8.4371(3), 12.9887(4), 20.6947(7)
α, β, γ (°)	101.205(3), 90.880(3), 102.562(3)
V (Å^3)	2167.45(13)
Z	4
μ (mm^{-1})	1.65
F(000)	1004
Data collection	
Radiation source	Enhance (Cu) X-ray source
h_{min}, h_{max}	−10, 9
k_{min}, k_{max}	−16, 16
l_{min}, l_{max}	−25, 25
T_{min}, T_{max}	0.768, 1.000
No. of independent refls.	8498
No. of observed [$I > 2s(I)$] refls.	4855
R_{int}	0.064
Refinement	
$R[F^2 > 2s(F^2)]$	0.034
$wR(F^2)$	0.074
S	0.94
No. of parameters	1189
H-atom treatment	H-atom parameters constrained
$\Delta\rho_{max}$, $\Delta\rho_{min}$ (e Å^{-3})	0.34, −0.27
Flack parameter	0.04 (3)

calculations with the use of Becke's three-parameters hybrid exchange–correlation functional (B3LYP) [16] incorporating B88 gradient-corrected exchange and Lee–Yang–Parr non-local correlation functional by means of quasi-relativistic LanL2DZ (Los alamos effective core pseudo-potential plus double-zeta) [17–19] basis set implemented in Gaussian 03 W program package [20]. Geometry optimization was achieved by the application of Berny optimization algorithm [21] without any symmetry restraint. The values of the convergence criteria in the optimization procedure are below 4.5×10^{-4} hartree/bohr for maximum force, 3.0×10^{-4} hartree/bohr for RMS force, 1.8×10^{-3} Å for maximum displacement, 1.2×10^{-3} Å for RMS displacement. To properly assign vibrational modes in the FTIR spectrum of the complex, frequency calculations were performed at the same level of theory, and then uniformly scaled by 0.972 [22].

Metalloaromaticity affects bond orders and geometrical parameters of metallacycles, therefore HOMA index [23] based on experimental bond lengths offer an opportunity for describing aromaticity levels of the metallacycles [24]. HOMA index describes the average squared deviation of bond lengths from an average value as follows;

$$\mathrm{HOMA} = 1 - \frac{1}{n}\sum_{j=1}^{n} \alpha_j \left(R_j - R_{opt}\right)^2, \quad (1)$$

where n is the number of bonds taken into the summation, R_j stands for a running individual bond length, α_j regarded as a normalization constant is equal to 257.7 for C–C, 93.52 for C–N and 157.38 for C–O bonds, fixed to give HOMA = 0 for nonaromatic Kekulé systems and HOMA = 1 for purely aromatic systems with all bonds equal to the optimal value $R_{opt} = 1.388$ Å for C–C, $R_{opt} = 1.334$ Å for C–N, $R_{opt} = 1.265$ Å for C–O [23].

4 Results and Discussion

4.1 Structure Determination of the Complex

The title compound whose a thermal ellipsoid view [25] of a symmetry-independent monomer is shown in Fig. 1 crystallizes in the triclinic space group $P1$ with four molecules in its asymmetric unit, i.e. complex A, B, C and D. While molecular site symmetry for complex B is C_{2v}, those of the others are C_2 [26]. Geometric parameters selected to describe coordination environment of the complex are given in Table 2. Depending on the substituent effects, coordination environments of certain Cu(II) or Ni(II) complexes containing Schiff base ligands [27] are varied from a square planar to a tetrahedral coordination geometry and show structural phase transitions by heating [28–33]. In the presence of polychelating ligands, coordination environment around Cu(II) metal center adopts a distorted square-planar geometry rather than a tetrahedron [34] as a result of multiple chelate ring strain around copper ion. The coordination geometry around copper in the 2+ oxidation state of the complex is established by the two phenolate oxygen atoms (O1 and O2) and the two imino nitrogen atoms (N1 and N2). In the asymmetric unit, while the shortest Cu···Cu distance is observed for complex A and B with inter-atomic separation of 3.591 Å, the distance between Cu centers of complex C and D is 5.570 Å.

Examination of the metal–ligand distances of Cu(II) Schiff base complexes [35–43] shows that the Cu–N distances are, in general, longer than those of Cu–O bonds as is in the title complex. Cu–N distances range from 1.930 to 2.020 Å, while the Cu–O distances have values between 1.870 and 1.931 Å. Cu–N and Cu–O distances of the

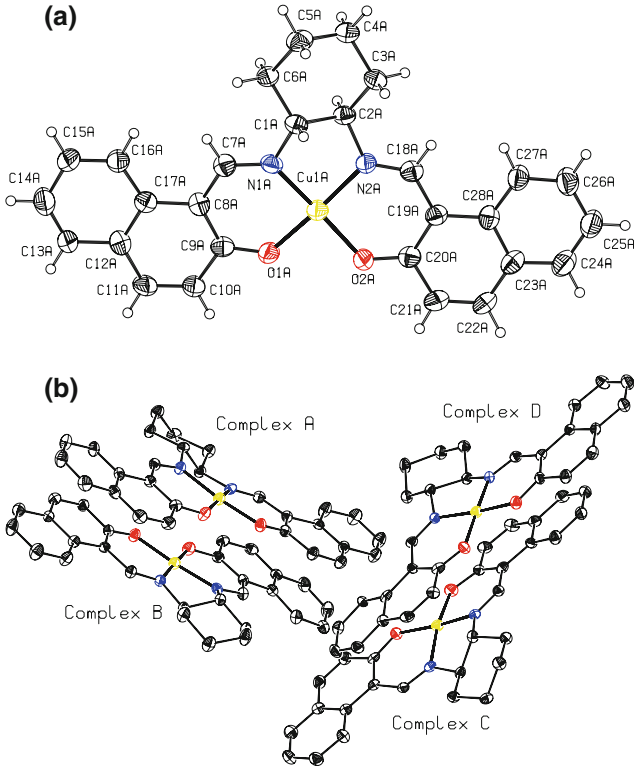

Fig. 1 **a** Thermal ellipsoid view of complex A with the atomic numbering scheme. Displacement ellipsoids are drawn at the 40% probability level and H atoms are shown as small spheres of arbitrary radii. An identical numbering scheme was applied to complex B, C and D. **b** Relative orientations of the monomers of the title complex in the asymmetric unit

complex are in the above ranges (Table 2). C7–N1 and C18–N2 imine bond lengths (Table 2) are also comparable with those observed in similar complexes [37, 38]. On the other hand, it is worth noting that the corresponding heteroatom bond lengths at opposite sides around twofold symmetry axis of the complex, i.e. Cu–N, Cu–O, C–O and C=N bonds (Table 2), are different from each other, due to different charge localization level as is in the pro-ligand [8]. In spite of this, bond lengths in the optimized geometry of the complex at opposite sides around twofold symmetry axis are almost identical as shown in Table 3. According to the results in Table 3, N–Cu–N angles are smaller than O–Cu–O angles for the title complex due to contraction from the polychelating property of the ligand. This tendency is observed for each monomer of the complex in the asymmetric unit as well.

4.2 Intramolecular Charge Transfer in the Complex

Levels of π-electron delocalization in naphthalene and chelate fragments of each complex are quantitatively expressed by their HOMA indices (Table 4). Loss in aromaticity of the ligand is quantitatively described as a summation of deviations in HOMA indices of both naphthalene fragments from HOMA index calculated for fully aromatic naphthalene (0.844) [44]. As can be seen from the results in Table 4, difference between the HOMA values of the naphthalene fragments in the same complex generally increases with increasing differences in the corresponding geometrical parameters at opposite sides of the symmetry axis of the complex (Table 2), since HOMA index defined by Eq. 1 describes the average squared deviation of bond lengths in a fragment from their optimal values in fully aromatic fragments. It is worth noting that π-delocalization levels of the chelate fragments including N1 and O1 is more than those including N2 and O2. As compared to the results in Table 3, it can be stated that electronic states or bonding situations in opposite sides of the twofold symmetry axis of the complex is different from each other as is in the pro-ligand of the complex [8]. Sequence of the loss in aromaticity of naphthene fragments or the amount of π-electron donation from the ligand to metal ion is found as A > C > D > B. As known, different electronic behaviors of the ligands can affect strongly oxidation state of the metal centers [9]. The loss in aromaticities of naphthalene fragments gives rise to enhanced aromaticity within metallacycles including imine bridge in the complexes. This electronic charge transfer is of great importance in the formation of the title complex. In order to progress the discussion in the above context, we need a further examination for the valences (or oxidation states) of copper ions in each complex.

To quantitatively evaluate oxidation states of Cu ion in the complexes, bond valence calculations were performed for each complex in the asymmetric unit (Table 5). The bond valences in the coordination environment were calculated as $v_{ij} = exp[(R_{ij} - d_{ij})/B]$ [45], where R_{ij} is the bond-valence parameter formally regarded as single bond between atom i and j [46], d_{ij} is the distance between the atom i and j, and B is equal to 0.37 [46, 47]. Here the bond-valence parameters for R_{Cu-N} and R_{Cu-O} were taken as 1.713 [46] and 1.679 [48], respectively. Total valance of Cu centers is determined by the valence summation rule [45]. In this regard, bond valence methodology may shed light on the relations between details of the coordination geometry and oxidation state of the metal center. The calculated bond valences are given in Table 5. It is well-known that the variation in the electronic state of metal center corresponds to certain changes in the covalent topology or equivalently geometric parameters of the electroactive ligand and vice versa [9]. As mentioned before, Cu–N bonds are, in general, longer than Cu–O bonds in Schiff base complexes, making the latter stronger than the former [40]. According to the results in Table 5, it can be stated that the deviation from formal oxidation state (2+) of Cu ion of the complex A is more pronounced than

Table 2 Selected geometrical parameters of the complex (Å, °) from X-ray crystallographic study

Bond lenghts					
Cu1A–N1A	1.901(7)	Cu1A–N2A	1.916(8)	Cu1A–O1A	1.880(6)
Cu1A–O2A	1.895(7)	C7A–N1A	1.30(1)	C18A–N2A	1.28(1)
C9A–O1A	1.29(1)	C20A–O2A	1.29(1)	C7A–C8A	1.42(1)
C18A–C19A	1.42(1)	C8A–C9A	1.41(1)	C19A–C20A	1.42(1)
Cu1B–N1B	1.919(8)	Cu1B–N2B	1.936(7)	Cu1B–O1B	1.898(7)
Cu1B–O2B	1.878(6)	C7B–N1B	1.31(1)	C18B–N2B	1.30(1)
C9B–O1B	1.31(1)	C20B–O2B	1.32(1)	C7B–C8B	1.44(1)
C18B–C19B	1.45(1)	C8B–C9B	1.39(1)	C19B–C20B	1.39(1)
Cu1C–N1C	1.925(8)	Cu1C–N2C	1.924(7)	Cu1C–O1C	1.897(7)
Cu1C–O2C	1.884(6)	C7C–N1C	1.29(1)	C18C–N2C	1.30(1)
C9C–O1C	1.31(1)	C20C–O2C	1.28(1)	C7C–C8C	1.42(1)
C18C–C19C	1.45(1)	C8C–C9C	1.43(1)	C19C–C20C	1.40(1)
Cu1D–N1D	1.924(7)	Cu1D–N2D	1.916(8)	Cu1D–O1D	1.880(7)
Cu1D–O2D	1.894(7)	C7D–N1D	1.28(1)	C18D–N2D	1.28(1)
C9D–O1D	1.31(1)	C20D–O2D	1.27(1)	C7D–C8D	1.41(1)
C18D–C19D	1.46(1)	C8D–C9D	1.42(1)	C19D–C20D	1.40(1)
Bond angles					
N1A–Cu1A–N2A	86.4(3)	O1A–Cu1A–O2A	88.1(3)	N1A–Cu1A–O1A	92.7(3)
N2A–Cu1A–O2A	93.6(3)	N2A–Cu1A–O1A	174.3(3)	N1A–Cu1A–O2A	172.1(4)
N1B–Cu1B–N2B	85.0(3)	O1B–Cu1B–O2B	87.5(3)	N1B–Cu1B–O1B	93.6(3)
N2B–Cu1B–O2B	94.1(3)	N2B–Cu1B–O1B	177.2(3)	N1B–Cu1B–O2B	174.9(3)
N1C–Cu1C–N2C	86.0(3)	O1C–Cu1C–O2C	89.8(3)	N1C–Cu1C–O1C	92.8(3)
N2C–Cu1C–O2C	92.9(3)	N2C–Cu1C–O1C	169.2(3)	N1C–Cu1C–O2C	171.6(3)
N1D–Cu1D–N2D	85.6(3)	O1D–Cu1D–O2D	87.9(3)	N1D–Cu1D–O1D	92.9(3)
N2D–Cu1D–O2D	93.8(3)	N2D–Cu1D–O1D	175.8(3)	N1D–Cu1D–O2D	177.4(3)

Table 3 Some selected geometrical parameters of the optimized geometry of the complex (Å, °) at DFT/LanL2DZ level

Bond lenghts					
Cu1–N1	1.969	Cu1–N2	1.969	Cu1–O1	1.928
Cu1–O2	1.928	C7–N1	1.320	C18–N2	1.320
C9–O1	1.321	C20–O2	1.321	C7–C8	1.434
C18–C19	1.434	C8–C9	1.439	C19–C20	1.439
Bond angles					
N1–Cu1–N2	85.61	O1–Cu1–O2	92.85	N1–Cu1–O1	91.15
N2–Cu1–O2	91.15	N2–Cu1–O1	172.49	N1–Cu1–O2	172.48

Table 4 HOMA indices of naphthalene and chelate fragments of the complexes in the asymmetric unit

Fragment	Complex A	Complex B	Complex C	Complex D
Napht. (C8 to C17)	0.4824	0.6952	0.6273	0.7309
Napht. (C19 to C28)	0.6543	0.8345	0.6392	0.6662
Loss in aromaticity of naphths.	0.5513	0.1583	0.4215	0.2909
N1, C7, C8, C9, O1	0.8737	0.7445	0.6855	0.7529
N2, C18, C19, C20, O2	0.7426	0.6330	0.6697	0.6222

those of the other complexes in the asymmetric unit. Valence of copper ions is ranked in the sequence of complex A > D > C > B and this is, in general, agreement with the sequence (A > C > D > B) of the loss in aromaticity level for naphthalene fragments in the complexes. Dependency of total valence at copper centers against the loss in aromaticity of naphthalene fragments is shown in Fig. 2. Linear correlation between them indicates that total valence of copper centers increases with increasing π-electron donation from naphthalene fragments. Thus,

Table 5 Calculated bond valences and total valences at copper centers (in valance units, v.u.) of the molecules in the asymmetric unit

	Molecule A	Molecule B	Molecule C	Molecule D
v(Cu–O1)	0.58086	0.55328	0.55478	0.58086
v(Cu–O2)	0.55778	0.58401	0.57462	0.55929
v(Cu–N1)	0.60163	0.57306	0.56385	0.56537
v(Cu–N2)	0.57773	0.54733	0.56537	0.57773
v(Cu)	2.31801	2.25768	2.25861	2.28326

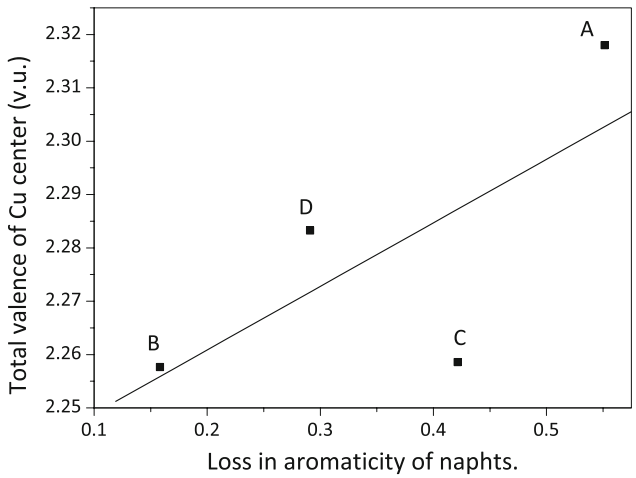

Fig. 2 Dependency of total valence at the copper center (y) against the loss in aromaticity of naphthalene fragments (x). Linear correlation is expressed by $y = 0.119x + 2.241$; $R^2 = 0.711$

intramolecular charge transfer mechanism has been elucidated by using structural parameters from X-ray crystallographic study. Naphthalene fragments in the complexes donate a part of their π-electrons to chelate fragments, and then these π-electrons are transferred into copper ions from chelate rings. Therefore, the title complex can be classified as ligand-to-metal charge transfer (LMCT) complex. It is worth noting that this intramolecular charge transfer through π-delocalized system in the ligand leads to metalloaromaticity within metallacycles including imine bridge.

4.3 Structural Evidence for Metalloaromaticity of the Complex

Establishment of the distorted square-planar coordination environments around copper centers is possibly not only due to polychelating ability of the pro-ligand, but also to an active electronic delocalization within the metal chelate rings referred to as metalloaromaticity [11]. A reasonable structural justification for metalloaromaticity property of the complex is the presence of π–π stacking interactions involving metallacycles. Castiñeiras et al. [49] reported that *N,N* type metallacycle in a copper (II) complex of 1,10-phenanthroline is involved in an intramolecular effective π–π stacking interaction between metallacycle and aryl ring. Similar interactions [49–51] have been described previously and strongly suggest an active electronic delocalization within the metallacycle. According to the results in Table 4, π-delocalization within metallacycles leads to a ring current and consequently to an electronic dipole moment. Dipole moments of such fragments interact with each other, leading to π–π interactions involving metallacycles with the aid of molecular stacking pattern in the crystal structure.

Although π–π interactions between aryl and metal-chelate ring are the first and well-known examples of structural evidences for metalloaromaticity [49], it has been recently put forward that π–π interactions between two metallacycles are a new class of structural evidence for metalloaromaticity [52]. As shown in Fig. 3, each complex in the asymmetric unit partakes in π–π interactions involving only chelate-metal rings. Thus, dimeric formations are constructed by the complexes in the crystal structure. Since complex A and B are related by twofold screw axis almost parallel to crystallographic $[2\,\bar{1}\,4]$ direction, molecular stacking pattern of them easily allows π–π interactions in the same asymmetric unit, whereas π–π interactions between complex C and D are observed in the neighboring asymmetric units due to a considerable amount of the slippage for them in the asymmetric unit as shown in Figs. 1b and 3. In the asymmetric unit, separations from Cg1A to Cg1B and from Cg2A to Cg2B are found as 3.464(5) Å and 3.636(5) Å, where Cg1 and Cg2 stand for the centroids of the respective mean planes

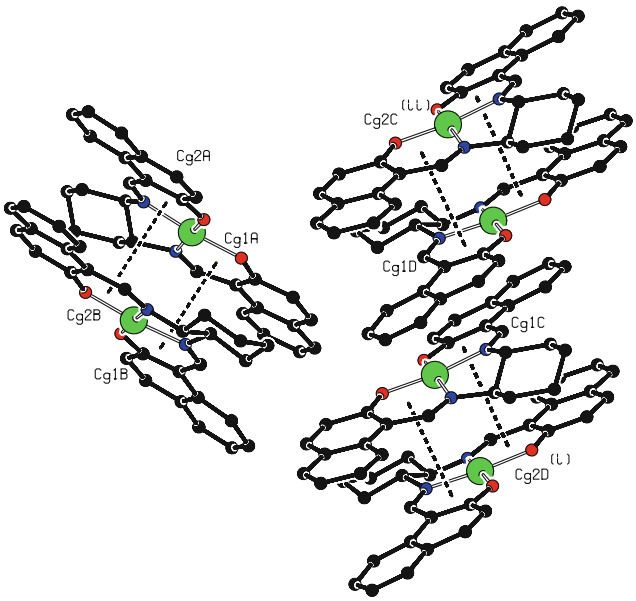

Fig. 3 π–π interactions involving metallacycles for the title complex. H atoms have been omitted for the sake of clarity

through metallacycles including N1/O1 and N2/O2. The distances from Cg1C at [x, y, z] to Cg2D at [(i): $x - 1$, y, z] and Cg1D at [x, y, z] to Cg2C at [(ii): $x + 1$, y, z] are found as 3.675(5) Å and 3.476(5) Å. Distances between the associated metal-chelate ring centroids presented here are acceptable as compared to their corresponding value of 3.62 Å reported in [52] for such interactions.

Considering aromaticity levels of metal-chelate rings given in Table 4, a complementary structural remark can be made: the more aromatic metallacycle pairs are involved in the stronger π–π interactions. Total aromaticity (1.6182) of Cg1A and Cg1B is more than total aromaticity (1.3756) of Cg2A and Cg2B, while total aromaticity (1.3077) of Cg1C and Cg2D is less than total aromaticity (1.4226) of Cg1D and Cg2C. The shortening centroid–centroid distance between the associated rings manifests the strength of $\pi\cdots\pi$ interaction. In this regard, it can be stated that the strength of $\pi\cdots\pi$ interaction increases with increasing π-electron delocalization level (or aromaticity) within metallacycle involving $\pi\cdots\pi$ interactions as shown in Fig. 4.

Dimerization between complex A and B becomes stronger by C1A–H1A···O1B and C1A–H1A···O2B weak intermolecular H-bonds as shown in Fig. 5a, while C2C–H2C···O1D$^{(i)}$, C2C–H2C···O2D$^{(i)}$ and C2D–H2D···O2C$^{(ii)}$ weak H-bonds given in Table 6 serve to stabilization of the dimeric formations between complex C and D as shown in Fig. 5b. Bifurcation bite angles, O1B···H1A···O2B and O1D···H2C···O2D, are found as 62.44(5)° and 63.08(4)°. Both types of dimeric formations are also linked to each other by C–H···π interactions whose geometric details are given in Table 6. These interactions serve to be strengthened the stacking of these dimers in the direction of a-axis giving rise to one dimensional polymeric arrangements.

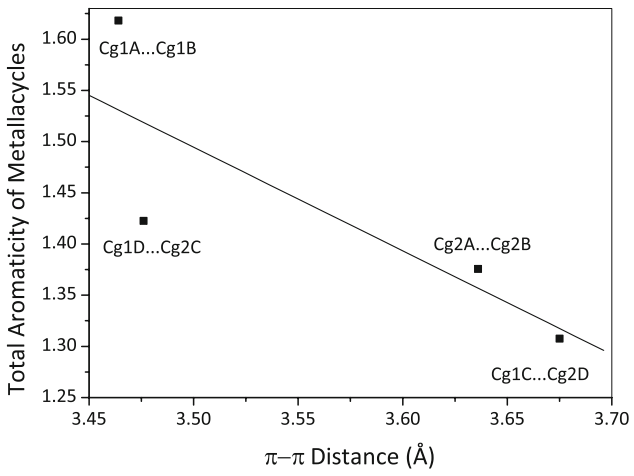

Fig. 4 Dependency of total aromaticity (y) of metallacycles involving π–π interactions against their centroid–centroid distances (x). Linear correlation is expressed by $y = -1.0117x + 5.03553$; $R^2 = 0.822$

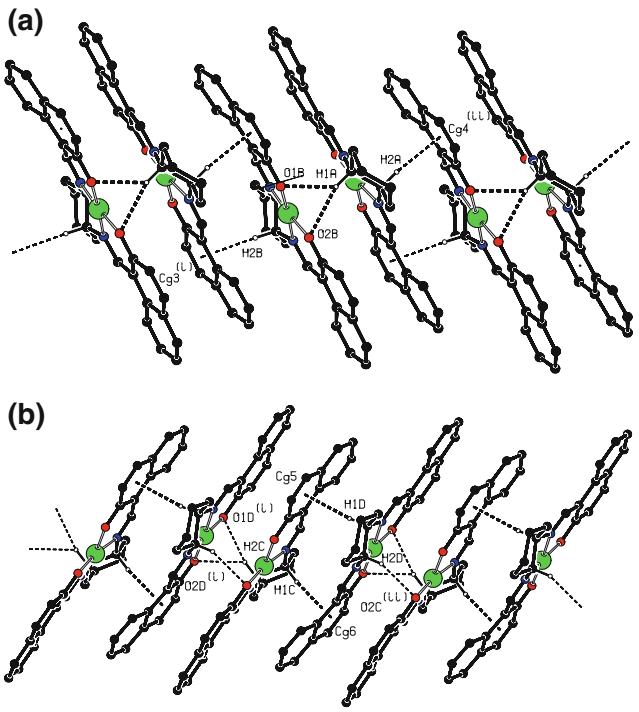

Fig. 5 Stacking of the dimers formed by complex pairs of A/B (**a**) and C/D (**b**) along a-axis. π–π interactions have omitted for the sake of clarity

Table 6 Geometric parameters (in Å and °) of intra- and intermolecular interactions of the title complex

D–H···A	D–H	H···A	D···A	∠D–H···A
C2B–H2B···Cg3$^{(i)}$	0.98	2.59	3.565(9)	177
C2A–H2A···Cg4$^{(ii)}$	0.98	2.48	3.457(8)	174
C1D–H1D···Cg5	0.98	2.57	3.540(8)	173
C1C–H1C···Cg6	0.98	2.50	3.473(8)	173
C1A–H1A···O1B	0.98	2.45	3.20(1)	133
C1A–H1A···O2B	0.98	2.58	3.493(9)	155
C2C–H2C···O1D$^{(i)}$	0.98	2.48	3.418(9)	160
C2C–H2C···O2D$^{(i)}$	0.98	2.53	3.21(1)	136
C2D–H2D···O2C$^{(ii)}$	0.98	2.41	3.30(1)	151

Cg3, Cg4, Cg5 and Cg6 stand for the centroids of the six-membered rings adjacent to metallacycles which include N2A/O2A, N1B/O1B, N1C/O1C and N2D/O2D, respectively

4.4 Vibrational Spectrum

Assignment of vibrational bands of Schiff base species is usually an arduous task because of the coupling several vibrational modes close to each other [53]. To cope with this problem, it is reasonable that quantum chemical calculations are performed to properly assign coupled vibrational modes besides pure ones. Experimental and calculated IR band assignments are listed in Table 7. FTIR spectrum of the title complex in Fig. 6 shows strong

Table 7 Comparison of the experimental and calculated vibrational spectra of the complex

Assignment	Scaled Wavenumber (cm^{-1})	Experimental Wavenumber (cm^{-1})	A (km/mol)
as. ν(Cu–O) + as. ν(Cu–N)	542.46	554.87	112.98
s. ω(CH) Ar.	763.37	740.10	119.09
θ(chxn.)	839.49	855.61	7.67
s. ω(CH) Ar. + $\delta(CH_2)$	850.44	829.01	129.16
as. ω(CH) Ar.	886.15	913.73	17.03
α(chxn.)	951.12	952.16	17.17
as. ω CH(Ar.) + $\delta(CH_2)$	965.81	979.90	19.90
ω(CH) imine + θ(naphth.) + as. ω(CH) Ar.	975.25	1037.54	35.69
$\nu(C_{methine}–N)$ + θ(naphth.)	1023.85	1091.87	15.33
$\delta(CH_2)$ + θ(naphth.)	1033.37	1142.57	32.00
γ(CH) Ar. + θ(naphth.) + as. ω(CH) Ar.	1089.11	1184.37	23.73
γ(CH) Ar.	1147.83	1212.41	5.88
γ(CH) Ar. + θ (naphth.) + $\delta(CH_2)$	1218.06	1247.54	68.05
as. $\omega(CH_2)$	1281.63	1309.63	59.23
as. $\omega(CH_2)$ + β(methyne) + γ(CH) Ar.	1297.98	1343.50	66.68
s. $\omega(CH_2)$	1339.59	1363.63	51.15
ν(C–O) + α(naphth.) + γ(CH) im.	1347.41	1395.90	427.26
γ(CH) Ar. + γ(CH) im. + ν(C=N) + s. $\omega(CH_2)$	1403.68	1433.47	252.50
γ(CH) Ar. + ν(C=N)	1430.26	1458.49	96.60
$\zeta(CH_2)$	1478.29	1506.27	13.65
ν(Ar. C=C)	1534.28	1540.62	216.34
ν(C=N) + ν(C=C) Ar.	1582.19	1618.21	691.16
ν(CH) methyne	2932.25	–	19.38
s. $\nu(CH_2)$	2951.57	2857.61	60.96
as. $\nu(CH_2)$	3020.59	2933.72	89.53
ν(C–H) im.	3086.28	–	29.29
ν(CH) Ar.	3126.06	3052.08	55.71

ν stretching, θ ring breathing, ω wagging, γ rocking, δ twisting, β bending, α skeletal, ζ scissoring, *s* symmetric, *as.* asymmetric, *naphth.* naphthalene, *Ar.* aromatic, *chxn.* cyclohexane, *im.* imine

absorption bands typical of Schiff-base complexes in the 1660–1500 cm^{-1} region which commonly could be attributed to ν(C=N) and ν(C=C) vibrations [54–61]. The band at 1618 cm^{-1} is not only due to C=N symmetric stretching mode but also to aromatic C=C vibrations as shown in Table 7. The results in Table 7 show that C=N symmetric stretching mode is strongly coupled with aromatic C=C stretching, CH rocking mode in neighboring imine and naphthalene fragments even with symmetric $–CH_2$-wagging in cyclohexane moiety. The band at 554.87 cm^{-1} in the IR spectrum of the complex can be assigned to the asymmetrical stretching vibrations of Cu–O and Cu–N bonds.

5 Conclusions

The methodology used in this work is essentially aimed at giving information about electronic charge transfer to be obtained from structural data for the title complex. Crystallographically independent four complexes have slightly different oxidation states at copper centers corresponding to different valence tautomeric states. In addition, bond valence calculations regarding metal ion based on experimental bond lengths provide a satisfactory quantitative tool for investigating differences valence situations at metal centers and furthermore, for detecting valence tautomerization levels as well. Naphthalene fragments in the complexes donate a part of their π-electrons to chelate fragments including imine bridge, and then these π-electrons are transferred into copper ions through chelate rings. Therefore, the title complex can be classified as ligand-to-metal charge transfer (LMCT) complex. Charge transfer mentioned above is verified by the correlation between total valence of copper centers and the loss in aromaticity of naphthalene fragments as shown in Fig. 2. Electron transfer through π-delocalized system in the ligand is essential in understanding its metallation ability and provides a useful chemical insight underlying metalloaromaticity of the complex. In the crystal structure, π–π interactions between metallacycles including imine bridge

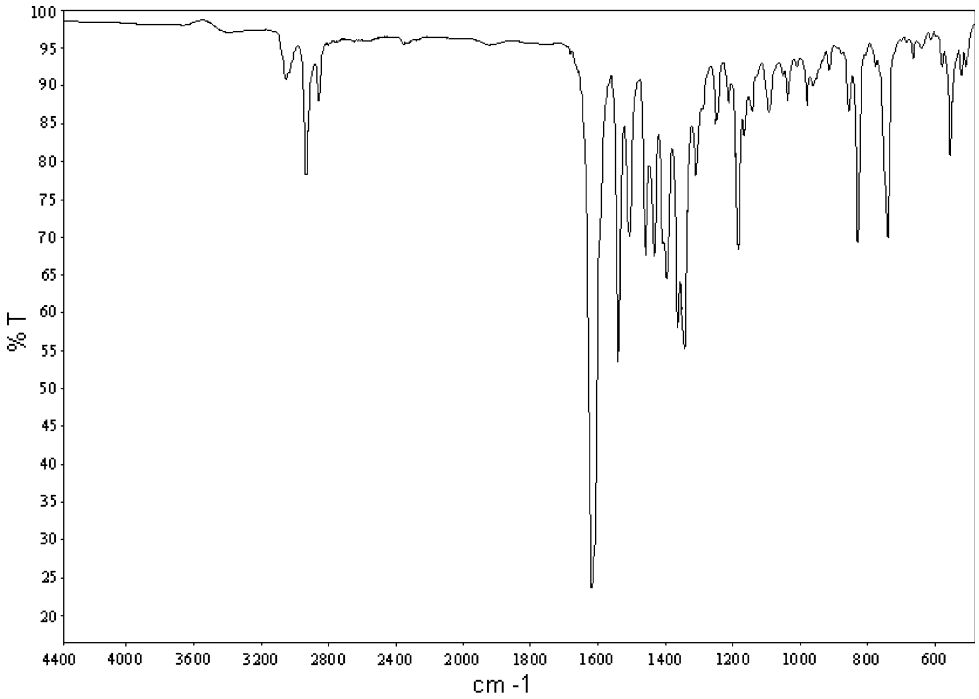

Fig. 6 FTIR spectra of the title complex

can be considered as a supporting evidence for metalloaromaticity in the complex. As shown in Fig. 4, decreases in the centroid–centroid distances of π–π interactions are associated with increased aromatic character of metallacycles including imine bridge. Dimeric formations between complex A and B besides C and D which are established by π–π interactions involving metallacycles are packed into one-dimensional polymeric arrangements generated by translation along the *a*-axis of the unit cell with the aid of C–H$\cdots\pi$ type interactions and strengthened by C–H$\cdots$O type bifurcated weak H-bonds in Fig. 5.

Acknowledgments Financial support from the Spanish Ministerio de Educacion y Ciencia (MAT2006–01997 and 'Factoría de Cristalización' Consolider Ingenio 2010), FEDER and Çukurova University Research Foundation (FEF2007BAP19) is gratefully acknowledged.

References

1. K.B. Borisenko, C.W. Bock, I. Hargittai, J. Phys. Chem. **100**, 7426 (1996)
2. H. Petek, C. Albayrak, M. Odabasoglu, I. Senel, O. Buyukgungor, J. Chem. Crystallogr. **38**, 901 (2008)
3. H. Karabiyik, N. Ocak-Iskeleli, H. Petek, C. Albayrak, E. Agar, J. Mol. Struct. **873**, 130 (2008)
4. H. Karabiyik, H. Petek, N.O. Iskeleli, C. Albayrak, Struct. Chem. **20**, 1055 (2009)
5. A. Filarowski, A. Kochel, M. Kluba, F.S. Kamounah, J. Phys. Org. Chem. **21**, 939 (2008)
6. L. Sobczyk, S.J. Grabowski, T.M. Krygowski, Chem. Rev. **105**, 3513 (2005)
7. P.M. Dominiak, E. Grech, G. Barr, S. Teat, P. Mallinson, K. Wozniak, Chem. Eur. J. **9**, 963 (2003)
8. H. Karabiyik, B. Guzel, M. Aygun, G. Boga, O. Buyukgungor, Acta Crystallogr. **C63**, o215 (2007)
9. E. Evangelio, D. Ruiz-Molina, Eur. J. Inorg. Chem. 2957 (2005)
10. O. Sato, J. Tao, Y.-Z. Zhang, Angew. Chem. Int. Ed. **46**, 2152 (2007)
11. H. Masui, Coord. Chem. Rev. **219**, 957 (2001)
12. J. Poater, M. Duran, M. Solà, B. Silvi, Chem. Rev. **105**, 3911 (2005)
13. Oxford Diffraction Ltd, *CrysAlis CCD and CrysAlis RED (Version 1.171.32.5)* (Abingdon, Oxfordshire, England, 2006)
14. L.J. Farrugia, J. Appl. Cryst. **32**, 837 (1999)
15. G.M. Sheldrick, Acta Crystallogr. **A64**, 112 (2008)
16. R.H. Hertwig, W. Koch, Chem. Phys. Lett. **268**, 345 (1997)
17. P.J. Hay, W.R. Wadt, J. Chem. Phys. **82**, 270 (1985)
18. P.J. Hay, W.R. Wadt, J. Chem. Phys. **82**, 284 (1985)
19. P.J. Hay, W.R. Wadt, J. Chem. Phys. **82**, 299 (1985)
20. M.J. Frisch, G.W. Trucks, H.B. Schlegel, G.E. Scuseria, M.A. Robb, J.R. Cheeseman, J.A. Montgomery, T. Vreven Jr., K.N. Kudin, J.C. Burant, J.M. Millam, S.S. Iyengar, J. Tomasi, V. Barone, B. Mennucci, M. Cossi, G. Scalmani, N. Rega, G.A. Petersson, H. Nakatsuji, M. Hada, M. Ehara, K. Toyota, R. Fukuda, J. Hasegawa, M. Ishida, T. Nakajima, Y. Honda, O. Kitao, H. Nakai, M. Klene, X. Li, J.E. Knox, H.P. Hratchian, J.B. Cross, C. Adamo, J. Jaramillo, R. Gomperts, R.E. Stratmann, O. Yazyev, A.J. Austin, R. Cammi, C. Pomelli, J.W. Ochterski, P.Y. Ayala, K. Morokuma, G.A. Voth, P. Salvador, J.J. Dannenberg, V.G. Zakrzewski, S. Dapprich, A.D. Daniels, M.C. Strain, O. Farkas, D.K. Malick, A.D. Rabuck, K. Raghavachari, J.B. Foresman, J.V. Ortiz, Q. Cui, A.G. Baboul, S. Clifford, J. Cioslowski, B.B. Stefanov, G. Liu, A. Liashenko, P. Piskorz, I. Komaromi, R.L. Martin, D.J. Fox, T. Keith, M.A. Al-Laham, C.Y. Peng, A. Nanayakkara, M. Challacombe, P.M.W. Gill, B. Johnson, W. Chen, M.W. Wong, C. Gonzalez, J.A. Pople, *Gaussian 03W, Revision C.02* (Gaussian, Inc, Pittsburgh, PA, 2003)
21. H.B. Schlegel, J. Comput. Chem. **3**, 214 (1982)
22. M. Pagliai, L. Bellucci, M. Muniz-Miranda, G. Cardini, V. Schettino, Phys. Chem. Chem. Phys. **8**, 171 (2006)

23. T.M. Krygowski, J. Chem. Inf. Comput. Sci. **33**, 70 (1993)
24. A. Crispini, M. Ghedini, J. Chem. Soc., Dalton Trans. 75 (1997)
25. A.L. Spek, *PLATON: A Multipurpose Crystallographic Tool* (University of Utrecht, The Netherlands, 2001)
26. T. Pilati, A. Forni, J. Appl. Cryst. **33**, 417 (2000)
27. S. Yamada, Coord. Chem. Rev. **190–192**, 537 (1999) and references therein
28. J.M. Fernandez, O.L. Ruiz-Tamirez, R.A. Toscano, N. Macias-Ruvalcaba, M. Aguilar-Martinez, Trans. Met. Chem. **25**, 517 (2000)
29. A. Castineiras, W. Hiller, J. Strahle, J. Romero, R. Bastida, A. Sousa, Acta Crystallogr. **C46**, 770 (1990)
30. T.P. Cheeseman, D. Hall, T.N. Waters, Nature **205**, 494 (1965)
31. P.L. Orioli, L. Sacconi, J. Am. Chem. Soc. **88**, 277 (1966)
32. H. Nozaki, H. Takaya, S. Moriuti, R. Noyori, Tetrahedron **24**, 3655 (1968)
33. G.-P. Li, Q.-C. Yang, Y.-Q. Tang, Y.-D. Guan, Z.-H. Shang, Acta Chim. Sinica **45**, 421 (1987)
34. A.C.W. Leung, M.J. MacLachlan, J Inorg Organomet Polym, Mater. **17**, 57 (2007)
35. Y. Elerman, A. Elmalı, S. Özbey, Acta Crystallogr. **C54**, 1072 (1998)
36. Y. Elerman, M. Geselle, Acta Crystallogr. **C53**, 549 (1997)
37. Y. Kani, S. Ohba, T. Ishikawa, M. Sakamoto, Y. Nishida, Acta Crystallogr. **C54**, 191 (1998)
38. J.M. Lo, H.H. Yao, F.L. Liao, S.L. Wang, T.H. Lu, Acta Crystallogr. **C53**, 848 (1997)
39. R. Kilincarslan, H. Karabiyik, M. Ulusoy, M. Aygun, B. Cetinkaya, O. Buyukgungor, J. Coord. Chem. **59**, 1649 (2006)
40. M. Ulusoy, H. Karabiyik, R. Kilincarslan, M. Aygun, B. Cetinkaya, S. Garcia-Granda, Struct. Chem. **19**, 749 (2008)
41. I. Castillo, J.M. Fernandez-Gonzalez, J.L. Garate-Morales, J. Mol. Struct. **657**, 25 (2003)
42. T. Akitsu, Y. Einaga, Polyhedron **24**, 2933 (2005)
43. A.A. Khandar, K. Nejati, Polyhedron **19**, 607 (2000)
44. J. Oddershede, S. Larsen, J. Phys. Chem. A **108**, 1057 (2004)
45. M. O'Keeffe, N.E. Brese, Acta Crystallogr. **B47**, 192 (1991)
46. M. O'Keeffe, N.E. Brese, J. Am. Chem. Soc. **113**, 3226 (1991)
47. I.D. Brown, D. Altermatt, Acta Crystallogr. **41**, 244 (1985)
48. C. Srivanavit, D.G. Brown, J. Am. Chem. Soc. **98**, 4447 (1976)
49. A. Castiñeiras, A.G. Sicilia-Zafra, J.M. González-Pérez, D. Choquesillo-Lazarte, J. Niclós-Gutiérrez, Inorg. Chem. **41**, 6956 (2002)
50. K. Molčanov, M. Ćurić, D. Babić, B. Kojić-Prodić, J. Organomet. Chem. **692**, 3874 (2007)
51. M. Ghedini, I. Aiello, A. Crispini, M. La Deda, Dalton Trans. 1386 (2004)
52. J.J. Fernández, A. Fernández, M. López-Torres, D. Vázquez-García, A. Rodríguez, V. Varela, J.M. Vila, J. Organomet. Chem. **694**, 2234 (2009)
53. I. Majerz, T. Dziembowska, Spectros. Lett. **42**, 246 (2009)
54. Y.-L. Zhang, W.-J. Ruan, X.-J. Zhao, H.-G. Wang, Z.-A. Zhu, Polyhedron **22**, 1535 (2003)
55. F. Gao, W.-J. Ruan, J.-M. Chen, Y.-H. Zhang, Z.-A. Zhu, Spectrochim Acta A **62**, 886 (2005)
56. R.N. Mohanty, K.C. Dash, Polyhedron **9**, 1011 (1990)
57. A. Pui, C. Policar, J.-P. Mahy, Inorg. Chim. Acta **360**, 2139 (2007)
58. H. Unver, A. Elmali, A. Karakas, H. Kara, E. Donmez, J. Mol. Struct. **800**, 18 (2006)
59. D.K. Dey, M.K. Saha, M.K. Das, N. Bhartiya, R.K. Bansal, G. Rosair, S. Mitra, Polyhedron **18**, 2687 (1999)
60. U.M. Rabie, A.S.A. Assran, M.H.M. Abou-El-Wafa, J. Mol. Struct. **872**, 113 (2008)
61. D.C. Ware, D.S. Mackie, P.J. Brothers, W.A. Denny, Polyhedron **14**, 1641 (1995)